Welding in the World (2023) 67:753–764
https://doi.org/10.1007/s40194-022-01444-9

RESEARCH PAPER

Experimental investigation on residual stress distribution in an austenitic stainless steel weld overlay pipe after local ultrasonic impact treatment

Chuan Liu[1] · Yuefeng Chen[2] · Hui Xiao[1] · Kai Wang[1] · ShuangWang[2] · Weihua Liu[2]

Received: 18 July 2022 / Accepted: 8 December 2022 / Published online: 20 December 2022

Abstract
A 304 stainless steel weld overlay pipe was manufactured, and the nickel-base alloy was applied as the overlay weld. The local region of the pipe was treated using ultrasonic impact treatment (UIT). The surface stresses were measured by the hole-drilling method, and the full map internal stresses were measured by the contour method. The effects of local UIT and overlay on the stresses in the overlay pipe were investigated. Results show that the local UIT induces a compressive stress layer in the treated region with a depth of about 2–3 mm. Weld overlay can extend the compressive stress depth at the weld zone, resulting in the compressive hoop stress at the weld centerline to a depth of 68–79% original girth weld wall thickness and compressive axial stress with a depth of 80% girth weld wall thickness.

Keywords Stainless steel pipe · Weld overlay · Welding residual stress · Ultrasonic impact treatment · Contour method

1 Introduction

Austenitic stainless steel piping systems, commonly joined by the fusion welding process, are important components in nuclear power plants. Austenitic stainless steel welded joints often suffer intergranular stress corrosion cracking (IGSCC) in the heat-affected zone (HAZ) of weldment because of environmental corrosion, material sensitivity, and applied tensile stresses [1, 2]. Due to the fast heating and cooling procedure of weld metal during welding, tensile residual stress is very likely to appear in the weld zone and stress concentration may occur in the weld toe and HAZ. It is well known that regions of compressive residual stress retard crack growth, while tensile residual stress regions lead to the contrary effect. Therefore, modification of welding residual stress in the weld zone, especially introducing the compressive stress, is very essential to mitigate the IGSCC. For piping components, the common stress mitigation methods, such as post-weld heat treatment [3] and mechanical stress improvement process [4], have limited effects in introducing beneficial compressive stress on the inner surface.

One effective strategy to mitigate IGSCC in stainless steel welded piping components is the full structural weld overlay [5]. It consists of weld metal laid over the outside diameter of the pipe in the girth weld region. Weld overlays are to provide several main benefits such as reinforcement of the cross-section of interest, prevention of possible leakage, and imposing compressive stress on the inner surface of the pipe [5]. It is also an important repair technique in the power generation industry, commonly being used for refurbishing low alloy steel piping systems suffering from IGSCC [6].

Understanding the residual stress distribution is critical for evaluating the reliability of pipe girth welds with weld overlay. Many studies have been extensively performed to understand the residual stress distribution in pipe girth welds with different materials after weld overlay. For example, residual stresses were determined through the thickness of a dissimilar weld overlay pipe using neutron diffraction by Woo et al. [7]. The results show significant changes in residual stresses induced by overlay from tension to compression

Recommended for publication by Commission XV - Design, Analysis, and Fabrication of Welded Structures

✉ Chuan Liu
chuanliu@fosu.edu.cn; mse.chuanliu@gmail.com

[1] School of Mechatronic Engineering and Automation, Foshan University, Foshan 528000, China

[2] China Nuclear Industry Fifth Construction Co., LTD, Shanghai 201400, China

through the thickness of the dissimilar weld overlay pipe specimen. Ren et al. [1, 8] measured the surface stress and through-thickness stress distribution in a 304 stainless steel weld overlay pipe with the hole-drilling method and the cutting-sectioning method. The pipes were butt welded together and overlaid with a 140-mm-long and 9-mm-thick weld overlay using 308L stainless steel welding filler metal. It was found that the axial and hoop residual stresses are compressive at the inner surface of the weld overlay pipe. Furthermore, the compressive stress distributes through most of the cross-section. Huang et al. [9] performed the structural integrity analyses for preemptive weld overlay on the dissimilar metal weld (DMW) of a typical pressurizer nozzle using the finite element (FE) method. It was confirmed that the residual compressive stress around the inside surface of the DMW has been shown to provide further mitigation of PWSCC degradation. Liu et al. [10] employed the FE analysis to investigate the post-overlay residual stress states in a DMW that joins the low alloy steel nozzle to the stainless steel safe end in a typical pressurized water reactor (PWR). This investigation has provided a reference for optimizing the weld overlay design of dissimilar metal welds in PWRs. Liu et al. [11] also conducted FE numerical studies for weld overlay on the feedwater nozzle to characterize the residual stress distribution. It was found that the residual stress is compressive after the weld overlay on the feedwater nozzle, which provides a more uniform and larger compressive axial and hoop stress region through the thickness. Zhang et al. [12] conducted detailed FE analyses to predict the stress variation during the essential fabrication steps of DMW nozzle and stainless steel welds at nuclear power plants. It was found that the tensile welding residual stress region was significantly reduced after the weld overlay, though tensile stresses still exist at regions of the DMW through the thickness. The radius-to-wall thickness ratio of the pipe, the width and length of the overlay, and the girth weld structure have effects on the stress distribution of the girth weld after weld overly. Therefore, the stress distributions in the girth weld after the weld overlay in ref. [11] are different from those in ref. [12].

Numerical simulations and experimental measurements are the main methods to investigate the residual stress distribution in the overlay weld piping component, as demonstrated in the above references. Experimental measurement is essential, as it provides the data to validate the accuracy of numerical simulation. On the other hand, validation of numerical predictions requires representative, closely characterized mock-ups with reliable and repeatable residual stress measurements [13]. However, the engineering scale components to be investigated are rare, because of the costs involved in their manufacture, the difficulties encountered in making reliable, diverse and repeatable residual stress measurements in large components, and the burden of detailed material property characterization required for reliable benchmarking of simulations [13]. Therefore, experiments on engineering scale components to get the full map of stress distribution are never too much for FE validation and deep comprehension of stress in these components.

Furthermore, experimental methods that can get sufficient and enough accurate results from a few but representative mockups are also demanded. The contour method (CM) proposed by Prime [14] is a relatively new but powerful stress measurement technique that can provide a detailed two-dimensional (2D) map of stress across a section of the measured component. It consists of cutting the sample and then measuring the deformation of the cut surface due to the stress release induced by cutting. The deformation of the cut surface is then used as the boundary conditions of a FE model to calculate the original residual stresses on the cut plane within the sample. The CM has been validated by comparing the stress results on weldments with neutron diffraction [15–18], high-energy synchrotron X-ray diffraction [19], slitting method [20], deep-hole method [21], and FE method [22–24]. It has often been applied to specimens whose large cross-sectional areas limit the applicability of neutron diffraction due to limited penetration [25, 26], and can now be applied to large-scale structures such as pipe butt welds [27–31] and thick welded joints [32]. The CM is not affected by composition changes, large grain size, and crystallographic texture that can compromise diffraction techniques. However, it is very sensitive to the quality of the cut and errors associated with plasticity caused by stress redistribution ahead of the wire during the cutting process [27]. Two random error sources are identified for the contour method. One is the uncertainty due to noise in the displacement surfaces (displacement error) and the other is the uncertainty arising from the smoothing of the displacement surfaces (model error) [33]. Besides, cutting-induced plasticity and bulge are systematic errors of the CM [24]. The contour method has enough measurement accuracy and can meet the requirement of scientific research and engineering application. Olson et al. [34] found that the total uncertainty of contour method measurement was related to the material elastic modulus (E) of the component to be measured, with a value of approximately $250\times10^{-6}\,E$ for the region within 1 mm of the component boundary and $125\times10^{-6}\,E$ for the interior. Even if the contour technique is destructive and large errors would appear at the edges (due to the difficulty to measure the true perimeter of the surface of interest), it is still the best one to give a complete 2D distribution of residual stresses across a section with large dimensions.

Though overlay weld has the effect of inducing compressive stress at the inner surface of the stainless steel pipe girth weld, tensile stress is also present throughout the thickness of the overlay weld itself. Especially the stress will abruptly change at the locations of the weld

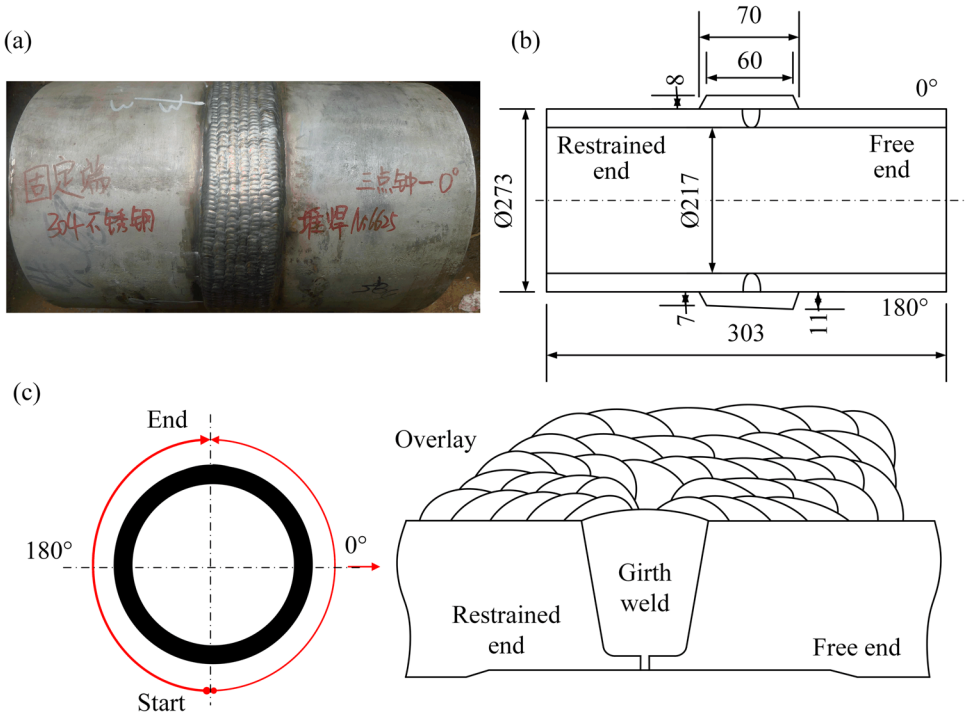

Fig. 1 (**a**) Photo of the weld overlay pipe; (**b**) dimensions of the weld overlay pipe; (**c**) schematic diagram of the overlay beads

Table 1 Compositions of the materials (wt. %)

	C	Mn	Si	Cr	Ni	Mo	Cu	Fe
304 stainless steel	0.068	1.1	0.5	17.1	8.2	-	-	Bal
ER308L weld metal	0.02	1.9	0.51	20.09	9.74	0.024	0.029	Bal
SNi6625 weld metal	0.011	0.15	0.04	21.5	64.14	8.98	0.01	0.31

start and end. The nuclear reactor piping system carries fluids with a certain pressure and the fluid pressure would fluctuate during the nuclear power plant operation, therefore the piping would experience the fatigue loads induced by the fluctuating fluids in the pipes. Large tensile stress, and surface imperfection in the overlay weld, as well as the fatigue loads, would be the cause of the fatigue crack initiation, and the crack would expand from the outer diameter side and the failure of the piping would happen. The fatigue of the piping system is also a matter of concern in nuclear power plants [9]. Accordingly, the large tensile stress in the weld overlay should be concerned. And it is helpful to mitigate the tensile stress in the weld overlay without affecting the already existing compressive stress at the inner surface. Therefore, stress mitigation methods with local effects are required. Ultrasonic impact treatment (UIT) is such a stress mitigation method [35]. It can induce a compressive stress layer with a depth of 2–4 mm in the treated zone without affecting the stress outside the impacted zone [31, 35]. In addition, the UIT-induced compressive stress has nothing to do with the initial stress state [36]. Besides, UIT is convenient to operate, and it provides the capability to treat hard-to-reach local areas and complex parts [37–39]. Accordingly, UIT is suitable for stress mitigation in local regions and engineering applications, especially the region with narrow operational space.

Table 2 Mechanical properties of the material

	Yield strength $R_{p0.2}$, MPa	Tensile strength R_m, MPa	Elongation A, %
304 stainless steel	280	590	49
ER308L weld metal	439	564	41.6
SNi6625 weld	420	760	30

Investigation of the effect of local UIT on the stress distribution of weld overlay pipe is helpful to extend the application of UIT and facilitate the UIT process optimization on the stress mitigation for local weld overlay. However, to the best of the authors' knowledge, there are few experiments on the stress distribution of weld overlay pipe with UIT. In the present study, a weld overlay pipe was fabricated first, then the UIT was applied to the

Table 3 Welding parameters for girth weld

Pass	Welding current *I*, A		Welding voltage *U*, V	Welding speed *v*, mm/min
	Peak	Base		
Root	120–170	50–60	9.8	70–80
Filling	220–280	100–140	10–10.5	60–75
Cap	230–240	110	10.3	50–60

local region of the pipe. The before and after UIT surface stresses of the weld overlay pipe were measured with the hole-drilling method. And the full maps of hoop stress on the weld cross-section and axial stress at the location of the weld centerline were obtained with the two-cut contour method. Moreover, the measurement procedure of the two-cut contour method for the large-scale pipe is introduced in detail. In our previous study, the as-welded stress in a girth weld without weld overlay was measured with the CM [30]. The girth weld in ref. [30] was prepared with the same pipe dimensions, groove configuration, and welding parameters as those of the girth weld with the weld overly in the present study. The effect of girth weld overlay on the through-thickness hoop and axial stresses at the weld centerline is distinguished with a comparison with the as-welded stress investigated in ref. [30]. The effect of local UIT on surface stress and internal stress is also investigated.

2 Materials and experimental procedure

2.1 Weld overlay specimen

Two 304 stainless steel pipes were butt welded together and overlaid with a 70-mm-long and 7–11-mm-thick weld overlay. The outer diameter and the thickness of the pipe are 273 mm and 28 mm, respectively. The photo of the weld overlay pipe, the dimensions of the overlay pipe, and the schematic diagram of the overlay beads are shown in Fig. 1.

The 308L stainless steel welding wire (1-mm diameter) was used to join the pipes with the narrow-gap pulsed gas tungsten arc welding (GTAW) technique and an automatic welding device. The nickel-base material is preferred for overlay weld in nuclear power stations due to its insensitivity to stress corrosion cracking. For example, the nickel-base weld overlay (Alloy 52 M) has been applied on the dissimilar metal weld (DMW) of a typical pressurizer nozzle [9], in which the attached piping is made of 304 austenitic stainless steel and 316L stainless steel. The nickel-base welding consumable is also used as the weld overlay on the boiling water reactors feedwater nozzle made of low alloy steel at a Taiwan domestic boiling water reactor [11]. Nickel-base overlay (Alloy 52 M) has been used for nuclear power plant nozzles made of low alloy steel and the safe end made of stainless steel [12]. In the present study, SNi6625 welding wire (similar to the ERNiCrMo-3 nickel-base welding wire) with a diameter of 2.4 mm was adopted to perform the overlay weld with the manual GTAW technique. Five weld layers in total are included in the weld overlay. The chemical compositions of 304 stainless steel, the girth weld metal, and the overlay weld metal are listed in Table 1 and the mechanical properties of the materials used in the present study are listed in Table 2. The welding parameters for the girth weld and overlay are shown in Table 3 and Table 4, respectively.

Table 4 Welding parameters for overlay weld

Current *I*, A	Voltage *U*, V	Welding speed *v*, mm/min
114–160	9.7–14.2	30–35

2.2 Ultrasonic impact treatment

To investigate the effect of local UIT on the welding residual stress in weld overlay pipe, UIT was applied to the weld overlay and its adjacent region in the 304 stainless pipes. The schematic diagram of the UIT-treated region on the weld overlay specimen is shown in Fig. 2a. The diagram of the UIT procedure, the UIT device used in the present study, and the photo of UIT on the overlay are shown in Fig. 2b and c. The driving frequency of the UIT device is 20 kHz and the impact frequency is about 180 Hz for the 4-mm-diameter 4-pin impact head. The UIT device was manually operated with an impact intensity of 12 s/mm^2 and 100% coverage to ensure the uniform indentation of the treated surface.

2.3 *Residual stress measurement*

2.3.1 *Surface measurement with the hole-drilling method*

The surface stresses of the weld overlay before and after UIT were measured with the hole-drilling (HD) method. The stress measurement line with the HD method is illustrated in Fig. 2a.

2.3.2 Two-cut contour method for internal stress measurement

The CM is employed to obtain the full map stress distribution on the cross-section of the weld overlay pipe. The residual stress map is determined by measuring the deformation on the cut surface. There are four steps involved in the CM: cutting the specimen into two parts; measuring the deformation contour of the cut plane and smoothening the contour data; building a FE model according to the dimensions of

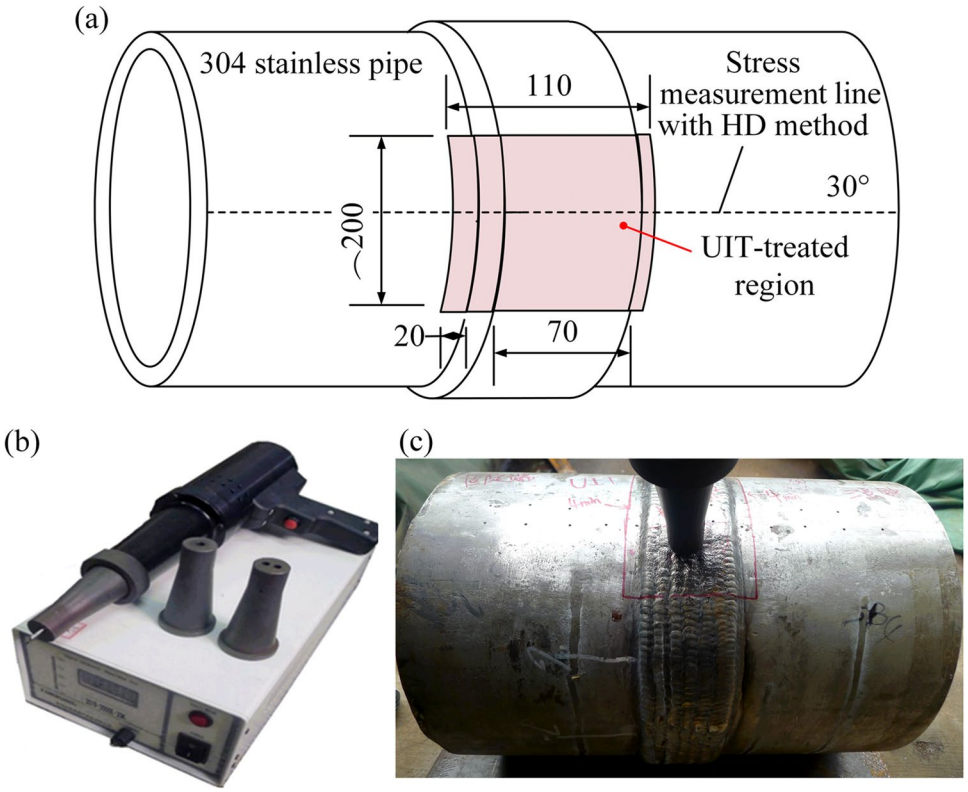

Fig. 2 (**a**) UIT-treated region; (**b**) UIT device; (**c**) UIT procedure

the after-cut specimen; and performing an elastic FE analysis using the smoothed deformation contour as the boundary conditions, finally, the original stress on the cut plane in the direction normal to the cut plane can be reconstructed. In the present study, two cuts were performed on the overlay pipe specimen, and the locations of the cut plane are shown in Fig. 3. After the first cut, the hoop stress distributions at 30° position (after-UIT stress) and 210° position (before-UIT stress) can be simultaneously obtained. After the second cut, the axial stress distribution along the weld line center can be constructed. At the weld line center, the local region of the overlay is treated with UIT and the rest remains untreated as shown in Fig. 3.

A Seibu M50A wire electrical discharge machining (WEDM) was used to perform a single flat cut along the cut plane using the skim cutting settings to achieve a cut surface with high-quality cutting. A special fixture was designed to clamp the pipe on the worktable of the WEDM. A pilot hole with a diameter of 0.5 mm was made using an electro-discharge drilling machine to provide self-restraint of the pipe to restrict the opening of the cut faces and thereby control the stress concentration and risk of plasticity at the cut

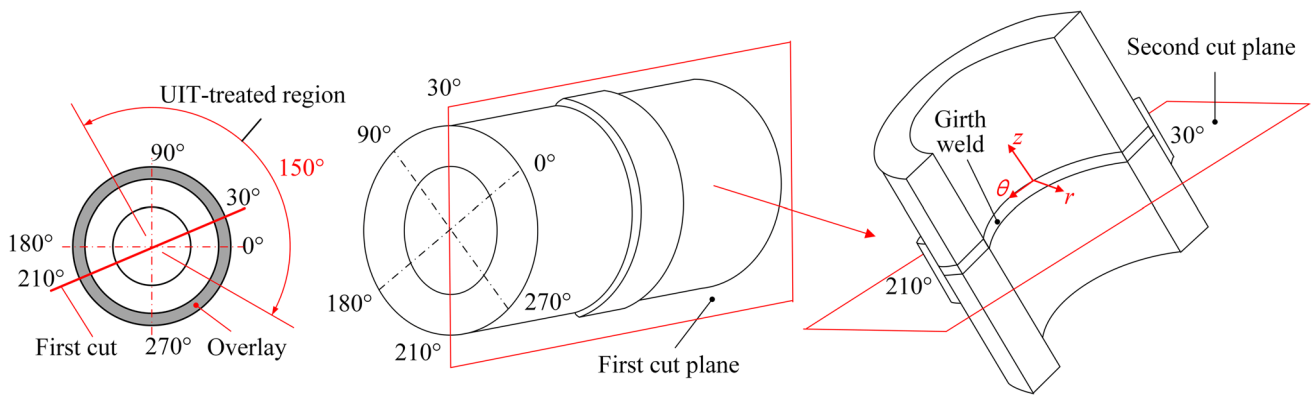

Fig. 3 Schematic diagram of the cut planes

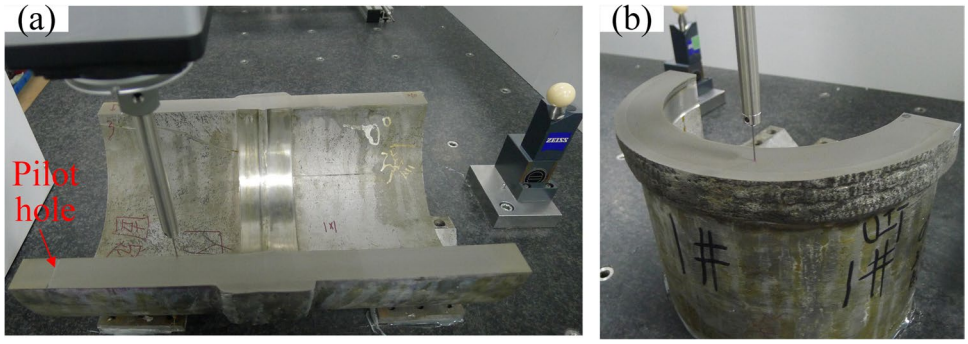

Fig. 4 (**a**) Contour measurement of the first cut plane; (**b**) contour measurement of the second cut plane

tip as well as prevent the pipe "springing open" owing to release of the hoop bending stress [29]. The brass wire of diameter 0.25 mm and cutting speed of about 0.15 mm/min was adopted to carry out the cuts.

After cutting, the displacements of the cut surfaces were measured using a Zeiss PRISMO ULTRA coordinate measuring machine (CMM) with a measurement space of 1 mm. The photos of the CMM measurement on the cut planes are shown in Fig. 4.

The deformation results of the two cut planes were processed by deleting the error points, interpolating the remaining points to a common grid, and averaging the data of the two cut planes. The averaged data were then smoothed using a bicubic spline fitting method. A FE model was established based on the dimensions of the after-cut specimen (half of the original specimen) using the commercial finite element software ANSYS with eight-node brick elements (Solid 185), and the smooth deformation data of the cut plane was applied to the FE model as the boundary conditions with additional boundary conditions to prevent the rigid movement of the model. Finally, the stress distribution on the cut plane was obtained through an elastic FE analysis. The obtained stress on the cut plane is that in the direction normal to the cut plane, that is, hoop stress distribution can be obtained on the first cut plane and the axial stress distribution can be obtained on the second cut plane. The FE models for the stress construction after the first cut and the second cut are shown in Fig. 5.

3 Results and discussion

3.1 Surface stress distribution measured by the hole-drilling method

The before-UIT and after-UIT surface stresses in the overlay weld and its adjacent region obtained by the hole-drilling method are shown in Fig. 6. As seen in the figure, the as-welded (AW) stress in the overlay weld is tensile stress ranging from about 100 to 350 MPa. The peak tensile stress occurs at the edge of the overlay weld. Outside the overlay weld, the tensile hoop and axial stress both drop to small tensile stress or compressive stress. After UIT, the tensile stresses in the treated region become compressive stresses ranging from – 560 to – 200 MPa. The after-UIT peak compressive stress is about – 560 MPa, which is larger than the yield strength of the nickel-base alloy weld metal. The after-UIT stress increase to a small tensile or

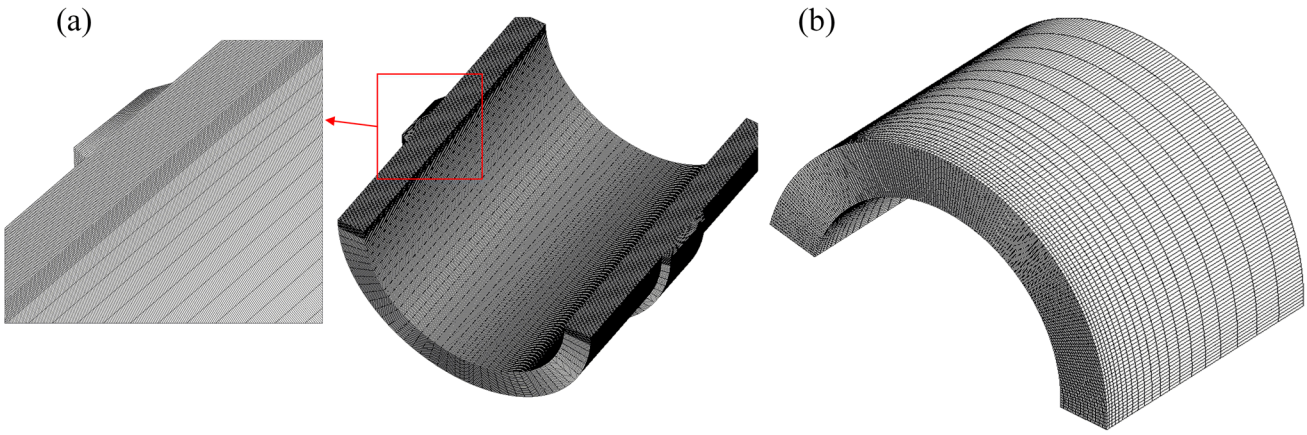

Fig. 5 FE models for the stress construction: (**a**) after the first cut; (**b**) after the second cut

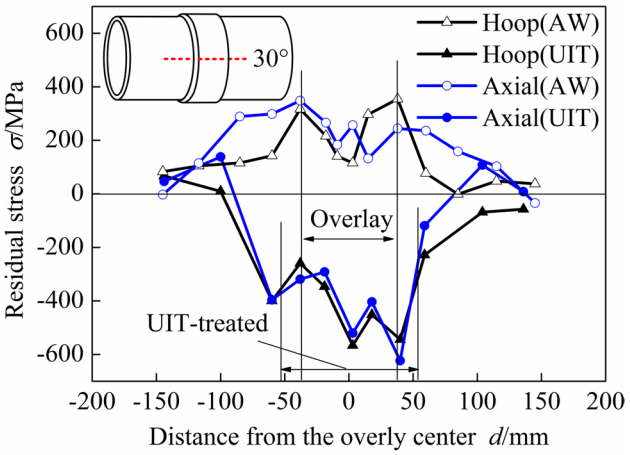

Fig. 6 Surface stress distribution measured by the hole-drilling method

compressive stress outside the impacted zone and close to the as-welded stress. It means that the UIT has little effect on the stress outside the impacted region. In addition, the after-UIT stresses in the treated region distribute more uniformly than the before-UIT stress; i.e., the after-UIT hoop stress has almost the same distribution and magnitude as the after-UIT axial stress. It can be inferred that the UIT has the same effect on the hoop and axial stresses in the nickel-base alloy overlay weld, and the after-UIT stress is independent of the initial as-welded stress. The effect of UIT on the welding stress in the nickel-base alloy weld in the present study is the same as that of UIT on the stresses in the low-alloy high-strength steel welds [35].

3.2 Hoop stress distribution obtained by CM

The hoop stress distribution on the first cut plane obtained by CM is illustrated in Fig. 7. It can be seen from Fig. 7 that compressive hoop stress ranging from – 300 to – 400 MPa appears near the inner surface in the girth weld zone. However, the as-welded hoop stress in the stainless steel girth weld (without weld overlay) is tensile near the inner surface as demonstrated in refs. [30, 31], in which the groove configurations, pipe dimensions, and welding processes are almost the same as those in the present study. Therefore, the experimental results in the present study confirm that overlay welding can introduce a compressive residual stress field at the inside surface of the girth weld. It can also be seen that the as-welded hoop stress (30° position) in the most region of the weld overlay is tensile (the hoop stress through all overlay thickness stays in tension), while the hoop stress in the region of weld overlay processed by UIT (210° position) is compressive stress with a certain depth. It means that the UIT can mitigate the welding stress in the nickel-base alloy weld overlay and introduce a compressive stress layer.

To further investigate the hoop stress distribution, six lines on the cut surfaces are selected and the hoop stresses along these lines are plotted and analyzed. The schematic diagram of the hoop stress evaluation lines is shown in Fig. 8. Lines L1 and L2 are located in the center of the girth weld and weld overlay. The through-thickness hoop stress without UIT (stress along line L1) and that with UIT (stress along line L2) can be evaluated. Lines L3 and L4 are the lines with a distance of 10 mm from the outer surface of the weld overlay (2-mm distance from the outer surface of the stainless steel girth weld). Lines L5 and L6 locate at a distance of 2 mm from the inner surface. Near-surface measurements with the contour method present additional noise in the data. The noise may be due to machining irregularities at the edge of the samples or introduced by the coordinate measuring machine's spherical tip going slightly past the edge of the part [14]. Therefore, the stress gradient at the surface tends to produce a large displacement gradient which is difficult to distinguish from the noise in the data

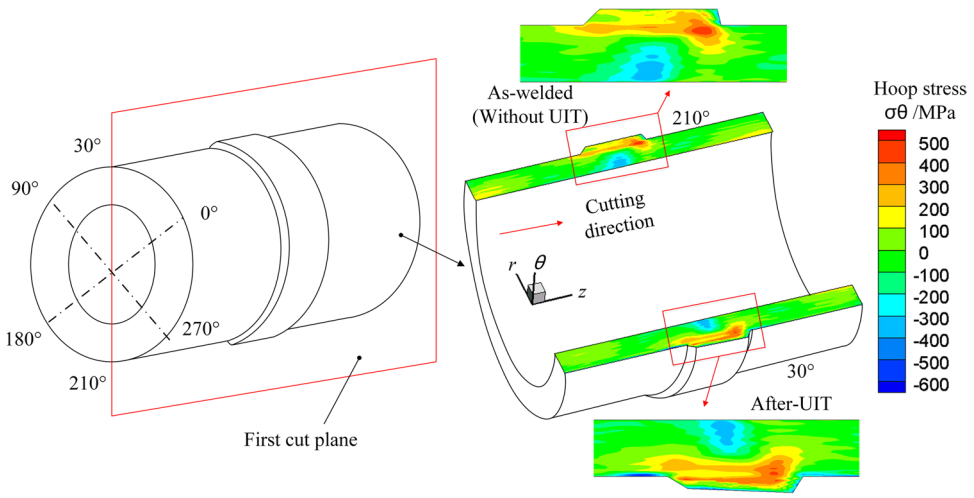

Fig. 7 Hoop stress distribution obtained by CM

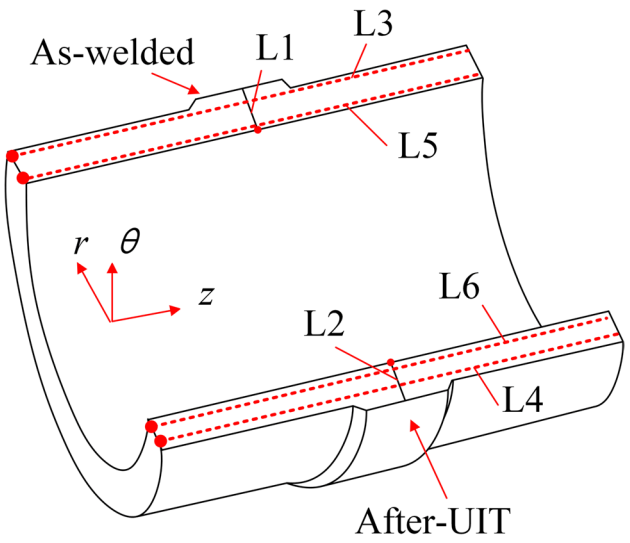

Fig. 8 Hoop stress evaluation lines on the first cut surfaces

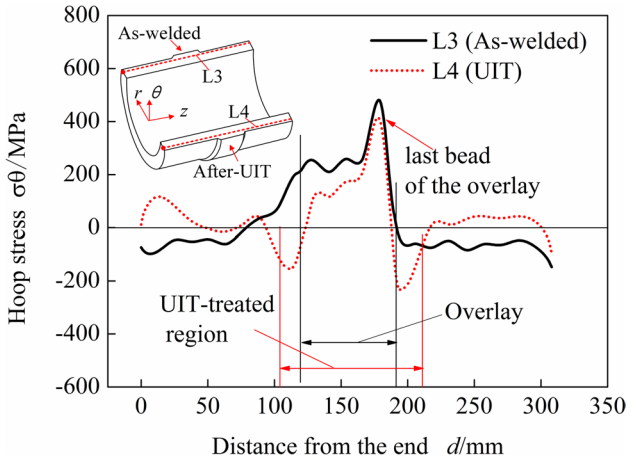

Fig. 10 Hoop stress distributions along lines L3 and L4

(surface roughness from cutting and measurement noise) [40], resulting in large uncertainty existing in the measured surface stress. Accordingly, the lines with a distance of 2 mm beneath the inner and outer surfaces (L3, L4, L5, and L6) are selected to evaluate the measured hoop stress in the present study. The hoop stresses along these lines are illustrated in Fig. 9, Fig. 10, and Fig. 11.

As seen from Fig. 9, large compressive stress with a magnitude of about − 500 MPa occurs near the outer surface of the region treated by UIT (line L2), while small value stress appears near the outer surface of the region without UIT (line L1). Except for the large difference (induced by UIT) occurring near the outer surface, the through-thickness hoop stress distributions along lines L1 and L2 demonstrate similar trends. In particular, the stress distribution trends and values along lines L1 and L2 are almost the same in the region towards the inner surface. It means that the UIT does not affect the hoop stress near the inner surface. As shown in Fig. 9, the compressive stress depth at the girth weld center from the inner surface is 22 mm (79% of the original girth weld thickness) and 19 mm (68% of the original girth weld thickness) along line L1 and line L2, respectively. The compressive stress near the inner surface of the girth weld in the present study is attributed to the overlay weld; therefore, the weld overlay can lead to compressive hoop stress near the inner surface to about 68 to 79% of the original girth weld thickness (28 mm). In addition, the peak compressive stress near the inner surface caused by the overlay weld is about − 380 MPa, which is close to the yield strength of the ER308L weld metal. It is also found that the UIT

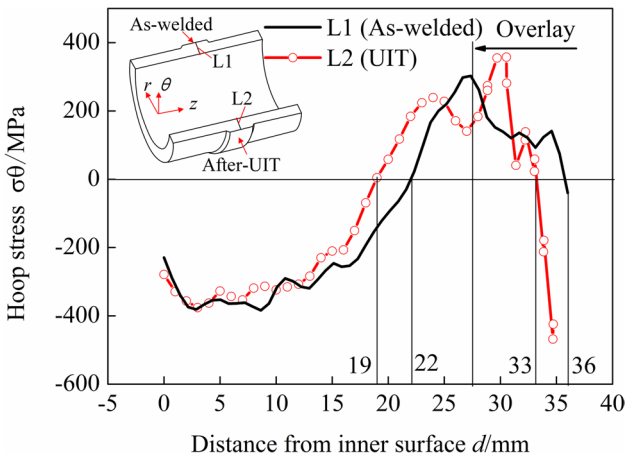

Fig. 9 Through-thickness hoop stress distribution along lines L1 and L2

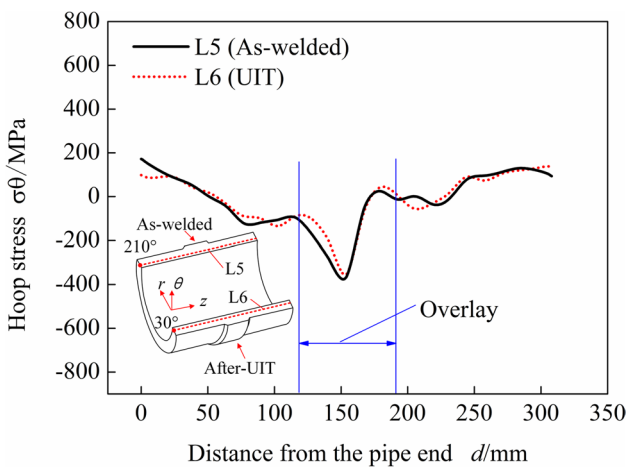

Fig. 11 Hoop stress distributions along lines L5 and L6

can induce a 3-mm-thick compressive stress layer in the nickel-base alloy weld overlay. Without UIT, the hoop stress through almost all overlay thickness stays in tension as indicated by the stress along line L1. The peak compressive hoop stress induced by UIT in the overlay is about – 500 MPa, which is higher than the yield strength of the weld overlay metal. The UIT-induced compressive stress near the outer surface of the overlay obtained by CM is close to that obtained by the hole-drilling method (shown in Fig. 6).

As seen in Fig. 10, the effect of UIT on the stress at the depth of 10 mm (lines L3 and L4) is not significant; therefore, the tensile hoop stress appears in the weld overlay at different locations along lines L3 and L4. The UIT region includes the overlay and its adjacent region of the stainless steel pipe as shown in Fig. 2a, and UIT can induce a compressive layer with a depth of 3 mm (as shown in Fig. 9); therefore, a compressive stress region appears near the overlay weld along the line L4 as compared with that along line L3. Generally, the hoop stress distribution trends in the weld overlay along lines L3 and L4 are similar. High tensile stress occurs on the right side of the overlay weld (the right side of the curve in the overlay region), which is the location of the final weld pass of the overlay.

As shown in Fig. 11, the hoop stress distribution along line L5 demonstrates almost the same as that along line L6. It can be deduced that local UIT on the overlay weld does not affect the stress near the inner surface of the pipe. It confirms that the stresses near the inner surface at 30° position and 210° position keep consistent after overlay. It can further be speculated that the hoop stress distribution is consistent all around the circumferential direction after overlay.

3.3 Axial stress distribution obtained by CM

The axial stress map at the girth weld center (the second cut plane) is shown in Fig. 12. As shown in Fig. 12, the as-welded axial stress through all overlay thickness stays in tension with a magnitude ranging from 100 to 300 MPa while a compressive stress layer with a magnitude of about – 200 to – 300 MPa appears in the overlay weld after UIT. Beneath the overlay, the axial stress in the girth weld is compressive. From Fig. 12 and Fig. 7, it can conclude that the UIT has the same effect on the stresses in both hoop and axial directions, inducing a compressive stress layer to a certain depth in both directions.

To have a quantitative comparison of the axial stress, five lines on the second cut plane are selected and line plots are developed to demonstrate the stresses along these lines. The schematic diagram of the stress evaluation lines is shown in Fig. 13. Lines L7 and L8 are located in the

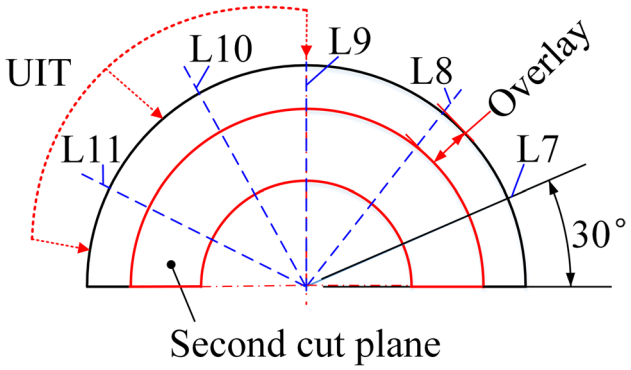

Fig. 13 Schematic diagram of through-thickness axial stress evaluation lines

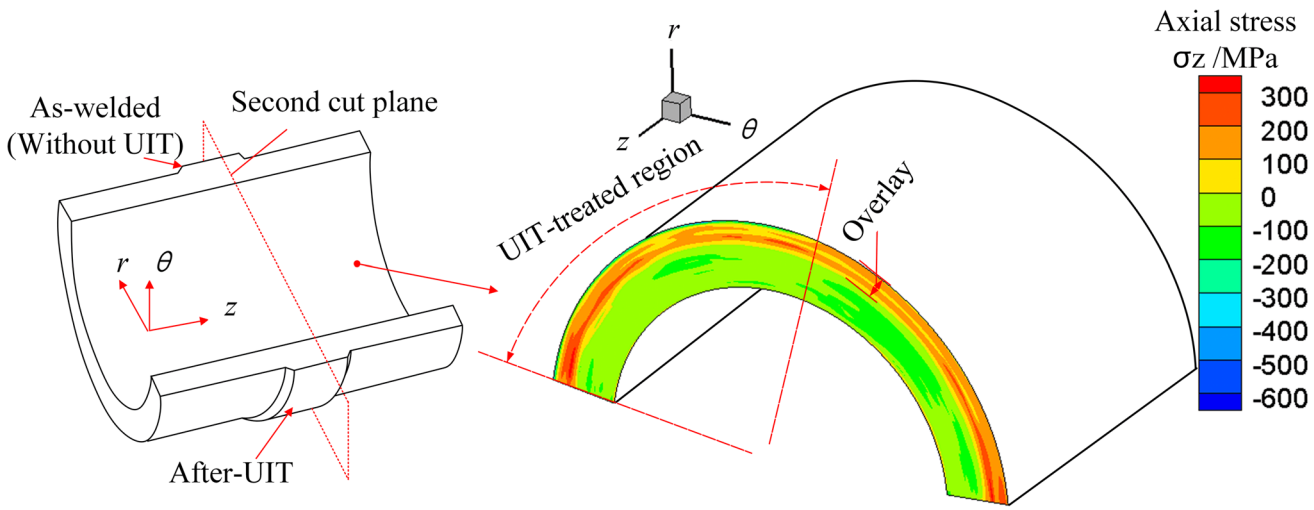

Fig. 12 Axial stress distribution on the second cut plane

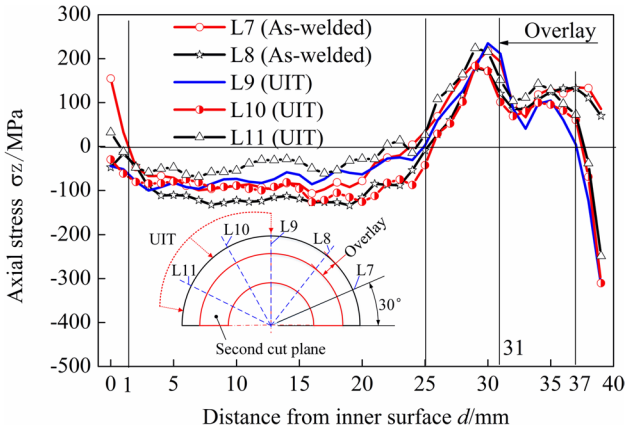

Fig. 14 Axial stress distributions along stress evaluation lines

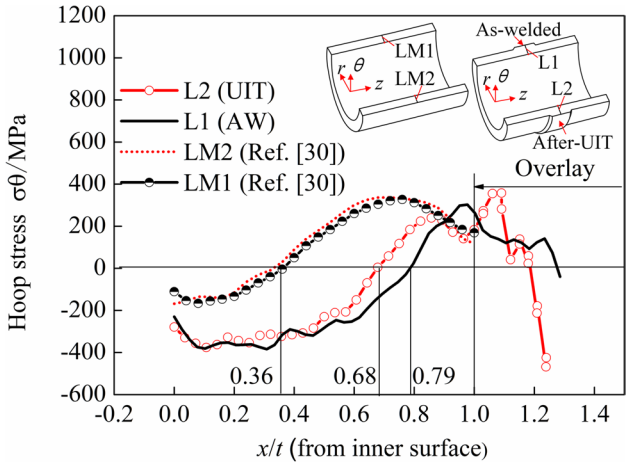

Fig. 15 Comparison of the through-thickness hoop stress at weld centerline between the overlay pipe and the girth weld

region without UIT, and lines L9, L10, and L11 are located in the UIT-treated region. The axial stresses along these lines are plotted in Fig. 14. Because of the axial shrinkage of pipe during girth weld butt welding, the girth weld metal near the inner surface is extruded out of the groove, resulting in an enlarged wall thickness at the weld centerline (the original wall thickness of the pipe before welding is 28 mm, while it is about 31 mm at the weld centerline after welding).

From Fig. 14, it can be seen that the tensile stress with a magnitude ranging from 70 to 250 MPa is present in the region of the untreated overlay weld, while the surface stress in the region of the UIT-treated overlay presents compressive stress of about − 350 MPa and the depth of the compressive stress reaches 2 mm. Apart from the compressive stress in the surface layer of the UIT-treated overlay weld, the through-thickness axial stress at the weld center has similar distribution along each line. Considering the stress uncertainty that exists in the surface layer (about 1–2 mm) for CM stress measurement and without considering the stress in the region with a distance of 1 mm from the inner surface, the depth of compressive axial stress from the inner surface reaches about 25 mm. Moreover, the compressive axial stress at the weld center along each line demonstrates a gentle distribution; i.e., there is no significant stress gradient occurring in the compressive axial stress region.

3.4 Effect of weld overlay on the residual stress in girth weld

Two key parameters control through-thickness residual stress distributions in the pipe girth weld. One is the welding linear heat input–related parameter and the other is the component radius-to-wall thickness ratio (r/t) [41]. In ref. [30], the groove configurations and radius-to-wall thickness ratio (r/t) of the 316L stainless steel girth weld are the same as those in the present study. In addition, the heat input used in ref. [30] is close to that of the 304 stainless steel pipe girth weld investigated in the present study. The weld overlay is adopted to mitigate the welding residual stress in the present study; therefore, the through-thickness stress distribution in these pipes can be used to distinguish the effect of overlay weld on the stress distribution in pipe girth weld. The through-thickness hoop stresses at the weld centerline from ref. [30] (without overlay) and those in the present study are demonstrated in Fig. 15. The through-thickness hoop stress in the girth weld is compressive stress towards the inner surface and tensile towards the outer surface at the weld centerline. The compressive stress depth at the weld centerline of the girth weld without overlay is about 36% of the original wall thickness from the inner surface, while in the overlay pipe, the zone of hoop compressive stress extends to about 68–79% of the original girth weld thickness from the inner surface. Therefore, the weld overlay leads to a larger depth of compressive hoop stress from the inner surface than the girth weld without weld overlay.

The through-thickness axial stresses at the weld center in the girth weld from ref. [30] are compared with those along lines L7 and L8 in the present study, as shown in Fig. 16. Without considering the axial stress near the inner surface (1-mm depth from the inner surface), the axial stress in the girth weld (without weld overlay) is compressive at the weld line center with a depth of 50–60% of the girth weld wall thickness from the inner surface [30]. This compressive stress depth is smaller than that in the overlay pipe in the present study (about 80% of the original girth weld wall thickness as shown in Fig. 16). In addition, the axial compressive stress at the weld line center in the overlay pipe distributes more uniformly as compared with the girth weld.

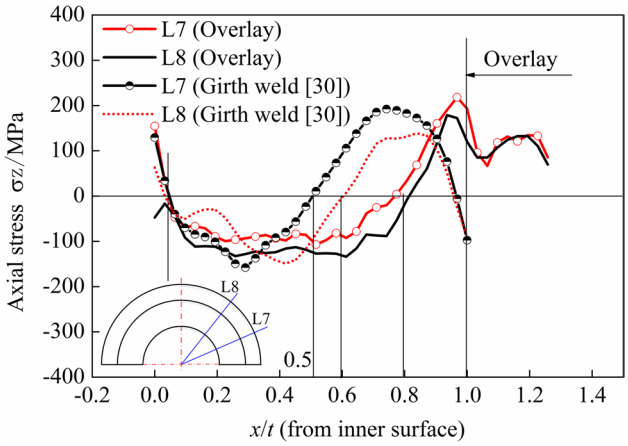

Fig. 16 Comparison of the through-thickness axial stress at weld centerline between the overlay pipe and the girth weld

From Fig. 15 and Fig. 16, it can be concluded that the overlay weld has the effect of improving the compressive axial and hoop welding residual stress fields in the region of the girth weld, providing additional compressive hoop and axial stresses to the pipe. The zone of compressive hoop stress in the overlay pipe extends to a distance of 68–79% through the pipe wall (at the weld centerline) compared with about 36% in the similar stainless steel girth weld. And the zone of compressive axial stress in the overlay pipe extends to 80% of the girth weld thickness from the inner surface compared with about 50–60% of the corresponding girth weld thickness without the overlay. It can also be seen from Fig. 16 that the overlay weld causes the compressive axial stress to be more uniform as compared with that in the girth weld. The results found in the present study are consistent with those found by Zhang et al. [12], in which the effects of weld overlay on stress distributions in the various pressurizer nozzle dissimilar metal welds (DMW) were investigated and it was found that the tensile stress region was reduced after the weld overlay, which provides a more uniform and rather large compressive axial and hoop stress region through the thickness.

4 Conclusions

(1) The surface stress of the nickel-base alloy weld overlay pipe is tensile stress with a magnitude ranging from about 100 to 350 MPa. The after-UIT surface stress in the treated region becomes compressive with a magnitude ranging from about − 560 to − 200 MPa. UIT induces almost the same distribution and magnitude of surface stresses in both hoop and axial directions in the treated region.

(2) Local UIT on the nickel-base alloy overlay induces a compressive stress layer in the treated region with a depth of about 2–3 mm, and it does not affect the stress near the inner surface of the overlay pipe.

(3) The zone of compressive hoop stress in the overlay pipe extends to 68–79% of the original girth weld wall thickness (at the weld centerline) compared with about 36% in the similar stainless steel girth weld.

(4) The zone of compressive axial stress in the overlay pipe extends to 80% of the original girth weld wall thickness from the inner surface compared with about 50–60% of the corresponding girth weld wall thickness (without weld overlay).

Funding This work is supported by the Research Foundation of China Nuclear Industry Fifth Construction (GYQJ2018-2–03-8), the Scientific Research Program for Young Talents of China National Nuclear Corporation (CNNC-2019–82), the Foshan Technology Project (1920001000409), and the Key Laboratory of Guangdong Regular Higher Education (2017KSYS012).

Declarations

Conflict of interest The authors declare no competing interests.

References

1. Yen HJ, Lin MCC (1995) Measurement of residual stress in the weld overlay piping components. Exp Mech 35:89–96
2. Guo X, He P, Xu K, Lv XCh, Zhang JB, ·Gu Y (2022) Microstructure investigation on the fusion zone of steel/nickel-alloy dissimilar weld joint for nozzle buttering in nuclear power industry. Weld World 66:187–194
3. Zhang T, Brust FW, Wilkowski G, Xu H, Betervide AA, Mazzantini O (2013) Welding residual stress in a large diameter nuclear reactor pressure vessel nozzle. J Pressure Vessel Technol 135(2):021208
4. Zhao T, Zhao Y, Wu A, Wang G, Yan D, Wan Z, Wu H (2021) Radial expansion approach and its mechanism to reduce residual stress and distortion of girth joint structure. J Manuf Process 70:214–224
5. Fredette LF, Scott PM, Brust FW, Csontos A (2010) An analytical evaluation of the full structural weld overlay as a stress improving mitigation strategy to prevent primary water stress corrosion cracking in pressurized water reactor piping. Proceedings of the ASME 2009 Pressure Vessels and Piping Division Conference. PVP2009–77327. July 26–30, 2009, Prague, Czech Republic. https://doi.org/10.1115/PVP2009-77327
6. Yildirim B, Nied HF (2004) Residual stresses and distortion in boiler tube panels with welded overlay cladding. J Pressure Vessel Technol 126(4):426–431
7. Woo W, Em V, Hubbard CR, Lee HJ, Park KS (2011) Residual stress determination in a dissimilar weld overlay pipe by neutron diffraction. Mater Sci Eng, A 528:8021–8027
8. Yen HJ, Lin MCC, Chen LJ (1996) Residual stress measurement in 304 stainless steel weld overlay pipes. J Eng Mater Technol 118:135–142

9. Huang CC, Liu RF (2012) Structural integrity analyses for preemptive weld overlay on the dissimilar metal weld of a pressurizer nozzle. Int J Press Vessels Pip 90–91:77–83
10. Liu RF, Wang JC (2021) Finite element analyses of the effect of weld overlay sizing on residual stresses of the dissimilar metal weld in PWRs. Nucl Eng Des 372:110959. https://doi.org/10.1016/j.nucengdes.2020.110959
11. Liu RF, Huang CC (2013) Welding residual stress analysis for weld overlay on a BWR feedwater nozzle. Nucl Eng Des 256:291–303
12. Zhang T, Brust FW, Wilkowski G, Huang CC, Liu RF, Ranganath S, Wang LH, Tsai YL (2012) Weld residual stress analysis and the effects of structural overlay on various nuclear power plant nozzles. J Press Vessel Technol 134(6):061205
13. Xiong Q, Smith MC, Muránsky O, Mathew J (2019) Validated prediction of weld residual stresses in austenitic steel pipe girth welds before and after thermal ageing Part 2: Modelling and validation. Int J Press Vessels Pip 172:430–448
14. Prime MB (2001) Cross-sectional mapping of residual stresses by measuring the surface contour after a cut. J Eng Mater Technol 123(2):162–168
15. Thibault D, Bocher P, Thomas M, Gharghouri M, Côté M (2010) Residual stress characterization in low transformation temperature 13%Cr–4%Ni stainless steel weld by neutron diffraction and the contour method. Mater Sci Eng, A 527(23):6205–6210
16. Woo W, An GB, ·Em VT, De ·Wald AT, Hill MR (2015) Through-thickness distributions of residual stresses in an 80 mm thick weld using neutron diffraction and contour method. J Mater Sci 50:784–793
17. Smith M, Levesque JB, Bichlera L, Sediako D, Gholipour J, Wanjara P (2017) Residual stress analysis in linear friction welded in-service Inconel 718 superalloy via neutron diffraction and contour method approaches. Mater Sci Eng, A 691:168–179
18. Braga DFO, Coules HE, Pirling T, Richter-Trummer V, Colegrove P, de Castro PMST (2013) Assessment of residual stress of welded structural steel plates with or without post weld rolling using the contour method and neutron diffraction. J Mater Process Technol 213:2323–2328
19. Frankel P, Preuss M, Steuwer A, Withers PJ, Bray S (2009) Comparison of residual stresses in Ti–6Al–4V and Ti–6Al–2Sn–4Zr–2Mo linear friction welds. Mater Sci Technol 25(5):640–650
20. Hosseinzadeh F, Toparli MB, Bouchard PJ (2012) Slitting and contour method residual stress measurements in an edge welded beam. J Pressure Vessel Technol 134(1):011402
21. Woo W, An GB, Kingston EJ, DeWald AT, Smith DJ, Hill HR (2013) Through-thickness distributions of residual stresses in two extreme heat-input thick welds: a neutron diffraction, contour method and deep hole drilling study. Acta Mater 61:3564–3574
22. Gadallah R, Tsutsumi S, Hiraoka K, Murakawa H (2015) Prediction of residual stresses induced by low transformation temperature weld wires and its validation using the contour method. Mar Struct 44:232–253
23. Muránsky O, Hamelin CJ, Hosseinzadeh F, Prime MB (2016) Mitigating cutting-induced plasticity in the contour method. Part 2: Numerical analysis. Int J Solids Struct 94–95:254–262. https://doi.org/10.1016/j.ijsolstr.2015.12.033
24. Muránsky O, Hosseinzadeh F, Hamelin CJ, Traore Y, Bendeich PJ (2018) Investigating optimal cutting configurations for the contour method of weld residual stress measurement. Int J Press Vessels Pip 164:55–67
25. Prime MB, Martineau RL (2002) Mapping residual stresses after foreign object damage using the contour method. Mater Sci Forum 404–407:521–526. https://doi.org/10.4028/www.scientific.net/MSF.404-407.521
26. Prime MB, Newborn MA, Balog JA (2003) Quenching and cold-work residual stresses in aluminum hand forgings: contour method measurement and FEM prediction. Mater Sci Forum 426–432:435–440. https://doi.org/10.4028/www.scientific.net/MSF.426-432.435
27. Mathew J, Moat RJ, Paddea S, Francis JA, Fitzpatrick ME, Bouchard PJ (2017) Through-thickness residual stress profiles in austenitic stainless steel welds: a combined experimental and prediction study. Metall Mater Trans A 48A(12):6178–6191
28 Smith MC, Muránsky O, Xiong Q, Bouchard PJ, Mathew J, Austin C (2019) Validated prediction of weld residual stresses in austenitic steel pipe girth welds before and after thermal ageing. Part 1: Mock-up manufacture, residual stress measurements, and materials characterisation. Int J Press Vessel Pip 172:233–250
29. Hosseinzadeh F, Bouchard PJ (2013) Mapping multiple components of the residual stress tensor in a large P91 steel pipe girth weld using a single contour cut. Exp Mech 53:171–181
30. Liu C, Wang JF, Wang S, Liu WH, Chen YF, Lin CH, Wang JX (2021) Experimental investigation on residual stress distribution in an engineering-scale pipe girth weld. Sci Technol Weld Joining 26(1):28–36
31. Liu C, Lin CH, Liu WH, Wang S, Chen YF, Wang JF, Wang JX (2021) Effects of local ultrasonic impact treatment on residual stress in an engineering-scale stainless steel pipe girth weld. Int J Press Vessels Pip 192:104420
32. Simoneau R, Thibault D, Fihey JL (2009) A comparison of residual stress in hammer-peened, multi-pass steel welds–A514 (S690Q) and S41500. Weld World 53:R124–R134
33. Olson MD, DeWald AT, Prime MB, Hill MR (2014) Estimation of uncertainty for contour method residual stress measurements. Exp Mech 55:577–585
34. Olson MD, DeWald AT, Hill HR (2018) Validation of a contour method single-measurement uncertainty estimator. Exp Mech 58:767–781
35. Liu C, Shen JB, Yan JL, Chu QL, Wang JX, Zhao Y (2020) Experimental Investigations on welding stress distribution in thick specimens after postweld heat treatment and ultrasonic impact treatment. J Mater Eng Perform 29(3):1820–1829
36. Liu C, Shen JB, Lin CH, Wang JF (2021) Effects of initial stress state on the subsurface stress distribution after ultrasonic impact treatment on thick specimens. J Strain Anal Eng Des 56(7):443–451
37. Yonezawa T, Shimanuki H, Mori T (2020) Influence of cyclic loading on the relaxation behavior of compressive residual stress induced by UIT. Weld World 64:171–178
38. Panin AV, Kazachenok MS, Kozelskaya AI, Hairullin RR, Sinyakova EA (2015) Mechanisms of surface roughening of commercial purity titanium during ultrasonic impact treatment. Mater Sci Eng, A 647:43–50
39. Vilhauer B, Bennett CR, Matamoros AB, Rolfe ST (2012) Fatigue behavior of welded coverplates treated with ultrasonic impact treatment and bolting. Eng Struct 34:163–172
40. Hatamleh O, Rivero IV, Swain SE (2009) An investigation of the residual stress characterization and relaxation in peened friction stir welded aluminum–lithium alloy joints. Mater Des 30:3367–3373
41 Song S, Dong P, Pei X (2015) A full-field residual stress estimation scheme for fitness-for-service assessment of pipe girth welds. Part I: Identification of key parameters. Int J Press Vessel Pip 126:58–70